Thesis for the Degree of Licentiate of Engineering

Evaluation of the Random-LOS Measurement System for Vehicular Communication Applications

Madeleine Schilliger Kildal

CHALMERS

Department of Electrical Engineering
Antenna Systems
Chalmers University of Technology

Göteborg, Sweden 2017

Evaluation of the Random-LOS

Measurement System for Vehicular Communication Applications

Madeleine Schilliger Kildal

Technical report number: R016/2017
ISSN 1403-266X

Department of Electrical Engineering
Antenna Systems
Chalmers University of Technology
SE–412 96 Göteborg
Sweden
Telephone: +46 (0)31 – 772 1000
Email: madeleine.kildal@chalmers.se

Front Cover: The figure on the front cover shows the Random-LOS test solution for vehicles.

Typeset by the author using LaTeX.

Chalmers Reproservice
Göteborg, Sweden 2017

Till pappa

Abstract

The automotive industry is progressively closing on the Telecom industry as wireless data connection and transmission become more and more important for vehicles. In both future and present cars, the safety and infotainment systems depend on reliable wireless data transmission. This is especially the case when autonomous cars will reach the market.

With this development, it becomes important to test and to verify that the required wireless communication is achieved. Today, there are no standardized methods of how to perform this testing. Proposed methods are all based on scaled up mobile phone testing. However, it is not problem-free to scale these methods to larger objects, such as vehicles, since it can become both expensive and complicated. To overcome these issues, a hypothesis has been introduced stating that *"If a wireless device is tested with good performance in both pure-LOS and RIMP environments, it will also perform well in real-life environments and situations, in a statistical sense"*. In this hypothesis, the Rich Isotropic Multipath (RIMP) and the Random Line-of-Sight (Random-LOS) are introduced as the two edge environments for testing. In this thesis, the focus is on one of these edge environments, i.e., the Random-LOS environment. This thesis studies how the Random-LOS environment can be realized for performance testing of wireless communication for vehicles.

The investigation has been divided in two main parts. The first is to study how the Random-LOS testing environment can be achieved. Simulations and measurements have been performed for three different chamber antennas, a single antenna element, a horizontal uniform linear array and a uniform planar array. The antennas have been compared in terms of amplitude (or rather power) and phase variations within a test zone in front of the chamber antenna.

The second part investigates how actual system performance measurements can be performed with a Random-LOS measurement setup. These measurements have been conducted with simplified setups, testing the concept and validate the throughput performance when comparing different vehicular antennas.

Keywords: Random Line-of-Sight, Rich Isotropic Multipath, Anechoic Chamber, Reverberation Chamber, Over-the-Air, car measurements, wireless communication, throughput.

Preface

This thesis is in partial fulfilment for the degree of Licentiate of Engineering at Chalmers University of Technology.

The work resulting in this thesis was carried out between September 2014 and December 2017 in the Antenna Systems group, Division of Communication and Antenna Systems at the Department of Electrical Engineering, Chalmers. Adjunct Professor Jan Carlsson has been the main supervisor and Assistant Professor Andrés Alayón Glazunov together with Associate Professor Jian Yang have been co-supervisors. Professor Thomas Eriksson has been the examiner.

The work presented in this thesis is financially supported by the Swedish Research Council (Vetenskapsrådet) as an industrial PhD project at Bluetest AB. The project is performed in collaboration with the company RanLOS AB.

Acknowledgment

The past three years have been an emotional rollercoaster with struggles I could never imagine but also with some of the nicest moments of my life. Thanks to all the supporting people around me, I have managed to conclude this thesis, which seemed like an impossible task one and a half year ago.

First I would like to thank my supervisor Adjunct Professor Jan Carlsson, for his great support and encouragement, and especially for always being there for me when I need a discussion partner. I also want to thank my co-supervisor Assistant Professor Andrés Alayón Glazunov for the time and interest you have put into my work. A thank also goes to my other co-supervisor Associate Professor Jian Yang, for being a good discussion partner. A special thanks goes to Professor Thomas Eriksson for examining this thesis.

I would also like to thank Bluetest, and especially John and Kjell for supporting me in difficult times and helping me to make the best of the situation. And to all the rest of you at Bluetest, welcoming me even though I am only at the office once a week.

I would also like to thank Lars for believing so much in me and making me grow as a person. Thank you Lars-Inge for always looking on the bright side of everything. And thank you Amir for helping me with the measurements and providing me with cars and antennas for doing my measurements.

I would like to thank all the colleagues at the department of Electrical Engineering and the antenna group, with a special thanks to the extended antenna family Abbas, Ahmed, Aidin, Astrid, Jinlin, Parastoo, Pegah, Tomas, Sadegh and Samar. You have all made everything easier, have been there through the hard times and have always made me laugh. A super thanks goes to Carlo and the best office mate in the world, Sadegh, for proof reading the thesis.

To Linnea, the best friend one could ever have. Thank you for always being there for me, always knowing when to call and what to say. And Josefin, thanks for being a great friend and the best pussel partner in the world. To Sten and Liv, we share the best combination of laughter, cries and deep talk. And to the rest of you, you know who you are, thank you!

Thank you amazing Carlo. So many things have happened these three years, and you have been there all along. I don't know what I would have done without you. You always know how to make me laugh, how to push me so that I challenge myself,

but also know when a hug is the best medicine in the world. Everything is easier with you.

To mum and Susanne. You are closest to my heart and mean the world to me. We have managed things together we didn't think were possible. We are a unit that can stand through anything.

To dad, I know you will read this somewhere, and I know you will be proud that I managed to do this. I am so happy that I started doing my PhD in your group, that I got to see your love and passion for your work every day, that I got to be a part of it, that I got to share it too. You have opened a fascinating world to me, and you inspire me every day. You will always be in my heart.

Madeleine
Göteborg, December 2017

List of Publications

This thesis is based on the work contained in the following appended papers:

Paper A
M.S. Kildal, J. Carlsson, and A.A. Glazunov, "Measurements and Simulations for Validation of the Random-LOS Measurement Accuracy for Vehicular Applications", submitted to *IEEE Transactions on Antennas and Propagation*, December 2017.

Paper B
M.S. Kildal, A.A. Glazunov, J. Carlsson, and A. Majidzadeh, "Evaluation of a Simplified Random-LOS Measurement Setup for Characterizing Antennas on Cars", in *2017 11th European Conference on Antennas and Propagation (EuCAP)*, 19-24 March, Paris, France.

Paper C
M.S. Kildal, J. Kvarnstrand, J. Carlsson, A.A. Glazunov, A. Majidzadeh, and P.-S. Kildal, "Initial Measured OTA Throughput of 4G LTE Communication to Cars with Roof-Mounted Antennas in 2D Random-LOS", in *2015 International Symposium on Antennas and Propagation (ISAP)*, 9-12 November, Hobart, Tasmania, Australia.

Paper D
M.S. Kildal, A.A. Glazunov, J. Carlsson, J. Kvarnstrand, A. Majidzadeh, and P.-S. Kildal, "Measured Probabilities of Detection for 1- and 2 Bitstreams of 2-port Car-roof Antenna in RIMP and Random-LOS", in *2016 10th European Conference on Antennas and Propagation (EuCAP)*, 10-15 April, Davos, Switzerland.

Paper E
M.S. Kildal, J. Carlsson, A.A. Glazunov, and P.-S. Kildal, "Measured LTE Throughput for SISO, SIMO and MIMO in Polarization-Random-LOS", in *2016 IEEE International Symposium on Antennas and Propagation (APSURSI)*, 26 June - 1 July, Fajardo, Puerto Rico.

Other related publications of the Author not included in this thesis:

- **M.S. Kildal**, X. Chen, P.-S. Kildal, and J. Carlsson, "Investigation of Mode Stirring with Plate on Platform in a Reverberation Chamber", in *2015 9th European Conference on Antennas and Propagation (EuCAP)*, 12-17 April, Lisbon, Portugal.

- A.A. Glazunov, P.-S. Kildal, J. Carlsson, **M.S. Kildal**, and S. Mansouri, "Impact of the Spatial User Distribution on the Coverage Antenna Pattern of Maximum Ratio Combining in Random Line-of-Sight", in *2015 9th European Conference on Antennas and Propagation (EuCAP)*, 12-17 April, Lisbon, Portugal.

- A.A. Glazunov, P.-S. Kildal, and **M.S. Kildal**, "Devising a Horizontal Chamber Array for Automotive OTA Tests in Random Line-Of-Sight", in *2015 International Symposium on Antennas and Propagation (ISAP)*, 9-12 November, Hobart, Tasmania, Australia.

- J. Kvarnstrand, S.S. Kildal, A. Skårbratt, and **M.S. Kildal**, "Comparison of Live Person Test to Head and Hand Phantom Test in Reverberation Chamber", in *2016 10th European Conference on Antennas and Propagation (EuCAP)*, 10-15 April, Davos, Switzerland.

Acronyms

5G	Fifth Generation mobile networks
AC	Anechoic Chamber
AoA	Angle of Arrival
AUT	Antenna Under Test
CDF	Cumulative Distribution Function
DUT	Device Under Test
EMC	Electromagnetic Compatibility
LOS	Line-of-Sight
LTE	Long Term Evolution
MIMO	Multiple-Input Multiple-Output
MISO	Multiple-Input Single-Output
MRC	Maximal-Ratio Combining
OTA	Over-The-Air
PEC	Perfect Electric Conductor
PoD	Probability of Detection
RC	Reverberation Chamber
Random-LOS	Random Line-of-Sight
RIMP	Rich Isotropic Multipath
SAE	Single Antenna Element
SIMO	Single-Input Multiple-Output
SISO	Single-Input Single-Output
TIS	Total Isotropic Sensitivity
TPUT	Data Throuhgput
TRP	Total Radiated Power
ULA	Uniform Linear Array
UPA	Uniform Planar Array
ZF	Zero Forcing

Contents

Part I

Introductory Chapters

Chapter 1

Introduction

Wireless connectivity in cars is becoming more and more important. The functionality of the cars depends on a reliable wireless communication, e.g., for safety systems, infotainment, traffic warnings and updates of software and maps. To ensure that the desired and required wireless communication is achieved, extensive testing needs to be performed. Today a lot of the testing is done with drive-tests out in the field. However, this is both expensive and can only be done late in the development process, which makes it hard to modify the product. Another problem with field-testing is that they are not repeatable, since the environment changes between measurements. This makes it difficult to identify the reason behind the changes in the results.

Thus exists the need to perform the testing in an earlier stage in the development, but also in a repeatable manner. No standardized method of how to do the testing of the wireless communication for vehicles exists today. Instead, wireless communication testing has been extensively investigated and developed in the mobile phone area. Different methods to perform mobile phone testing are, for example, described in the standardization documentation [1]. These methods include the Multiprobe Anechoic Chamber (MPAC), the two-stage method and the Reverberation Chamber (RC). However, it is not problem-free to adopt these methods for vehicle testing. There are issues with the size of the test object, as well as a different propagation environment for cars as compared to mobile phones.

In [2], a hypothesis states that, *"If a wireless device is tested with good performance in both pure-LOS and RIMP environments, it will also perform well in real-life environments and situations, in a statistical sense"*. This hypothesis introduces two edge environments, i.e., the Rich Isotropic Multipath (RIMP) and the Random Line-of-Sight (Random-LOS). These environments can be seen as as each others opposites, where the RIMP environment is based on an environment with many incoming signals, whereas in Random-LOS environment there is only one dominant random signal. Real-life propagation channels will lie in between these two channels.

1.1 Aim of the Thesis

The aim of the thesis is to investigate the Random-LOS environment and its possibilities and limitations for testing vehicular cellular communication. This has been done by dividing the study into two main parts.

The first part is to evaluate the field in the near-field region of the Random-LOS chamber antenna to find out if the desired field distribution, a plane wave, is achieved. This is done both through simulations and measurements. Comparisons between different type of chamber antennas have been made to find the most suitable option for the Random-LOS testing. The evaluations are mostly done in terms of standard deviation of the field amplitude within the test zone. The phase has also been analysed to see how well the plane wave behaviour is emulated.

The second part is to show how the Random-LOS test system can be used for active testing of the cellular communication for cars. This has been done for simplified Random-LOS measurement setups, where different antennas, mounted both on ground planes and on the roof of cars, have been evaluated in terms of data throughput. Both the random angle of arrival and polarization have been investigated. The performance has also been presented together with results in the RIMP environment to see how the two edge environments complement each other.

1.2 Thesis Outline

This thesis consists of two main parts. The first part contains five chapters and introduces the reader to the research topic, by giving relevant background information and presenting the main contributions. The second part includes the most relevant publications in full format. A detailed list of all the publications by the author, including non-appended publications, is given in the Section "List of Publications".

The first part of the thesis contains the following chapters. The first chapter, Chapter 1, gives a brief introduction to the topic and states the aim of the thesis. In Chapter 2, a background is given to give a better understanding of the following chapters. The background consists of an introduction to various antenna measurement techniques, both for determining traditional antenna design parameters, as well as measurements for characterizing wireless devices such as mobile phones. The real-world hypothesis is introduced together with the two edge environments, RIMP and Random-LOS. In this section it is also introduced the Random-LOS measurement setup for vehicles. The background also contains a brief introduction to wireless communication together with a description of the threshold receiver model used when processing the active Random-LOS measurement results. Chapter 3 describes measurements and simulations done to characterize the accuracy within the test zone in the Random-LOS measurement setup. In Chapter 4, measurements in a simplified Random-LOS measurement setup are presented for different vehicular antennas, as

well as a complementary measurements in a RIMP environment. The final chapter, Chapter 5, describes possible future work directions as well as a brief summary of the main contributions.

Chapter 2

Background

It is indispensable to evaluate the performance of antennas and wireless devices in order to achieve the desired system performance. There are different ways to do this, depending on where, i.e., in what propagation environment, and how, i.e., for what applications they are used. This chapter will give a background into different measurement techniques, both for traditional antenna parameters, but also for active testing of the wireless system performance of devices. This chapter will also describe the hypothesis for Over-the-Air (OTA) measurements of devices introduced in [2], and the Random Line-of-Sight (Random-LOS) and Rich Isotropic Multipath (RIMP) edge environments will be described more in detail. Some wireless communications basics together with the threshold receiver model [3] will be introduced as well.

2.1 Measurement Techniques

There exist different techniques to measure and evaluate the performance of antennas, depending on whether they are used as pure antennas, or integrated in active devices. Traditional antenna measurements are described in Section 2.1.1, whereas measurements for antennas used in mobile phones and other devices are described in Section 2.1.2.

2.1.1 Traditional Antenna Measurements

Traditionally, antenna performance parameters have been measured in anechoic chambers. These are based on passive measurements where, for example, the reflection coefficient, the far-field radiation pattern in E-, H-, or D-planes, the antenna directivity, gain as well as the beamwidth are systematically measured. These metrics are especially important to evaluate the performance of fix antennas, where the transmitter and receiver are directed towards each other.

Different techniques can be used to evaluate the performance parameters of traditional antennas. Among the most common ones are setups in free-space environments. In a free-space environment, the aim is to suppress all reflections, which is commonly realized in an Anechoic Chamber (AC). In ACs the walls, the floor and the ceiling are covered in RF-absorbing materials [4]. The performance metrics are obtained for the far-field of the measured antenna, where the field has a uniform amplitude and phase, i.e., it is locally a plane wave. There exist different ways to get the far-field performance and three of the most used ones are far-field ranges, near-field to far-field transformations and compact ranges [5, 6].

Far-field Range

As the name imply, the far-field ranges measure directly in the far-field of the antenna. This can be achieved if the source antenna and the Antenna Under Test (AUT) are placed far from each other, with a minimum distance, d, corresponding to the inner boundary of the far-field region

$$d = \frac{2D^2}{\lambda} \ , \tag{2.1}$$

where D is the largest linear dimension of the antenna and λ is the wavelength [5]. This can be realized most easily in an outdoor environment, since this can require very large distances. However, outdoors, there might be problems with reflections from the ground and surrounding objects, as well as problematic weather conditions impacting the measurement accuracy. Sometimes the required distances become even too large for an outdoor range, and other methods are therefore required.

Two different examples of far-field ranges are the elevated free-space range and the slant free-space range. The elevated free-space range, seen in Fig. 2.1, is designed such that the antennas are mounted at a sufficient height, to reduce unwanted ground reflections that can influence the measurement results. To further improve this, the source antenna is mounted such that the first null in the radiation pattern is directed towards the base of the tower [6]. In the slant free-space range, instead of elevating the source antenna, it is placed on the ground, while the AUT is still elevated. The source antenna is oriented such that the maximum of the radiation pattern points towards the center of the AUT and the first null is pointed towards the base of the AUT-tower to avoid the ground reflection.

Near-field to Far-field Transformation

Another way to get the far-field radiation pattern is to sample the near-field and then transform it into far-field values by Fourier transformation [7]. Both the amplitude and phase are sampled and it is usually done in a well defined grid with one of the following three shapes: a plane, a cylinder or a sphere in front of or around the AUT. The most complete is the spherical case, but it is also the most expensive one, since

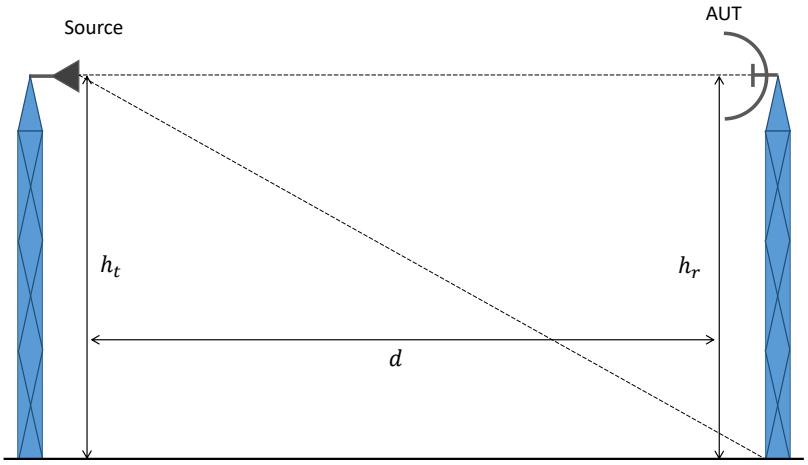

Figure 2.1: Elevated free-space range.

the positioning and probe equipment can become quite expensive. The measurements can be performed either by fixing the probe and rotating the AUT, or moving the probe around the fixed AUT [8]. Since the sampled near-field data has to be post-processed with numerical integration and Fourier transformation, no real-time data can be acquired by using a near-field to far-field transformation measurement method.

Compact Range

The far-field scenario requires that the AUT is illuminated by a plane wave. This can be realized in a compact range chamber, where a parabolic reflector usually is used to create a plane wave close to the AUT [9]. With this technique it is possible to make smaller indoor ranges that can be used to measure radiation patterns with high accuracy.

The reflector is illuminated by a feed antenna which, can be located directly in front of or offset from the reflector. The diverging rays from the feed antenna are collimated by the reflector and in front of the reflector the AUT is positioned [10]. A perfect plane wave cannot be achieved, since the reflector is finite in size and has an imperfect surface. The test zone where the AUT is placed in front of the reflector is called the quiet zone. This is the area where the amplitude and phase variations are small. Compact ranges typically provide a peak-to-peak phase variation of $\pm 5\,^\circ$ and a peak to peak amplitude variation of $\pm 0.5\,\mathrm{dB}$ in the quiet zone [11].

The reflector can operate in a large frequency band, as long as the feed is a wideband antenna. The lower frequency limit is determined by diffractions from the edges of the reflector, whereas the upper frequency limit is determined by the imperfections of the surface [10].

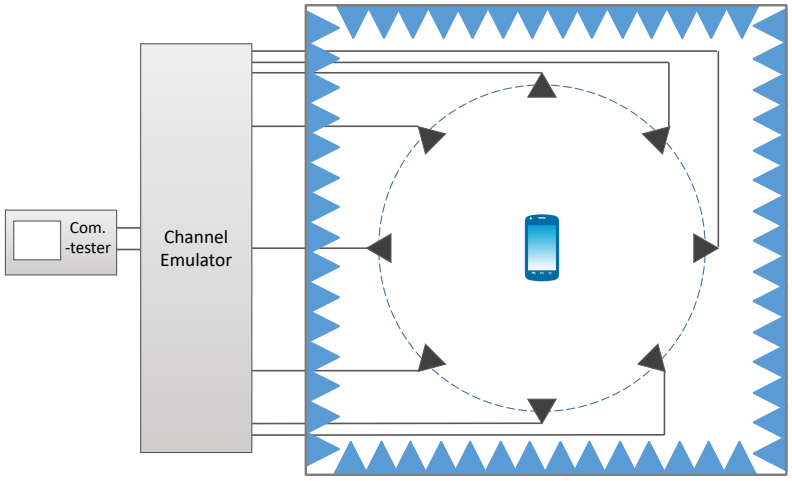

Figure 2.2: The Multiprobe Anechoic Chamber (MPAC) setup.

2.1.2 Mobile Phone Measurements

With the introduction of mobile phones there also came the need of testing their active wireless communication performance. This means the testing is performed on a system level, including the antenna and the device as a whole. Naturally, this must be done by means of Over-the-Air (OTA) tests, where no measurement cables, that can influence the antenna performance, are used. To perform a cable connected measurement on the antenna integrated in a mobile phone can be problematic for other reasons too. For example, there might not bee any designated or accessible test-connectors for connecting RF-cables to the antenna. The most common tests for evaluating the radiated performance of mobile phones are the ones that measure the Total Radiated Power (TRP) in the uplink, the Total Isotropic Sensitivity (TIS) and the data throughput in the downlink [12].

There are different methods used to test the active performance of mobile devices, such as mobile phones, tablets and laptops. Among the most common methods are the Multiprobe Anechoic Chamber (MPAC), the two-stage method and the Reverberation Chamber (RC).

Multiprobe Anechoic Chamber (MPAC)

The Multiprobe Anechoic Chamber (MPAC) setup is made up of a set of antenna probes positioned around the DUT in an anechoic chamber, see Fig. 2.2. The probes are usually placed in a 2D ring or 3D sphere, but can also be positioned in clusters [1]. The Device Under Test (DUT) is placed in a clearly defined test zone, which is in the center of the probes. In order to perform the measurement, a communication tester or base station simulator is connected to a channel emulator connected to the antenna probes. It is possible to transmit signals form different directions as the probes are

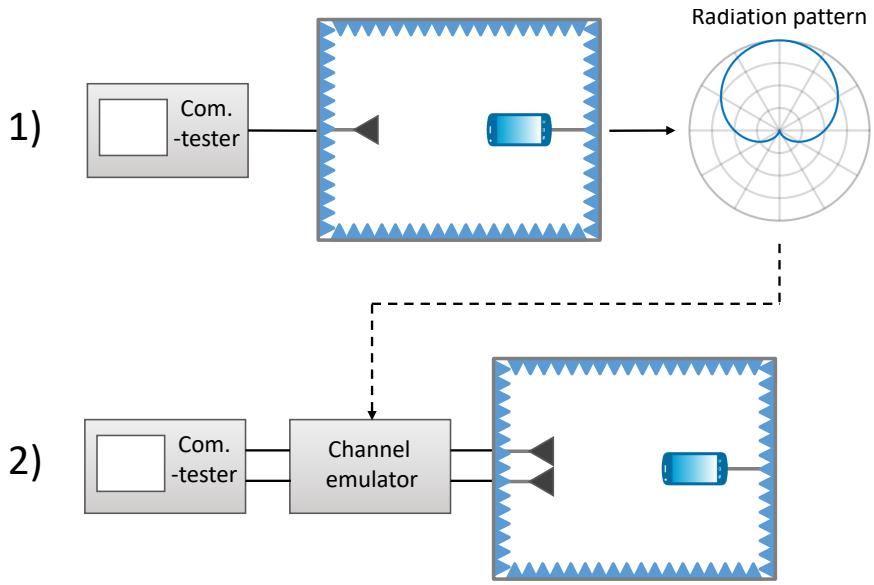

Figure 2.3: The radiating two-stage method. The first stage shows how the radiation pattern is obtained and the second stage show how the channel model is applied to the radiation pattern and fed to the DUT.

located in different positions. Different propagation and fading environments can be realized by emulating different channel models [13].

The number of probe antennas depends on the number of fading channels (one for each probe), the size of the test zone and whether the measurements are Single-Input Single-Output (SISO) or Multiple-Input Multiple-Output (MIMO). As a minimum amount, eight probes with a spacing of 45 °, are used for the ring solution, and at least three clusters must be used for the cluster version [1, 14]. Additional probes are needed if dual polarization is desired. A multiprobe setup for cars has been studied in [15].

Two-stage Method

The two-stage methods requires the execution of two subsequent measurement steps. In the first stage, the radiation pattern of the DUT is measured, and in the second stage, the desired channel model is applied to the radiation pattern. The resulting signal is fed to the DUT to emulate the desired communication link, see Fig. 2.3 [1,16].

The radiation pattern, in the first stage, can be acquired by simulations or by actual measurements performed on the device. To obtain the measured radiation patterns of the device, a built-in testing mode, to measure relative phase and amplitude in the device itself is needed. By calibrating the incoming signal, it is then possible to obtain the radiation pattern. These measurements are performed inside an anechoic chamber with a communication tester [17].

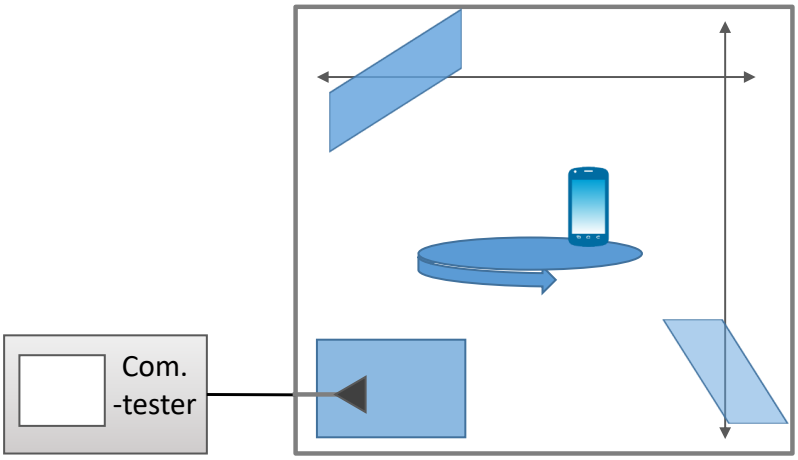

Figure 2.4: The reverberation chamber (RC).

In the second stage, the output of a communication tester is connected to the input of a channel emulator. In the channel emulator, the desired channel model is applied to the radiation pattern and this is then applied to the signal from the communication tester. The connection between the channel emulator and the DUT can be achieved either through a conducted or radiated mode. In the conducted case, RF-cables from the channel emulator are connected to the internal antenna ports on the DUT. On the other hand in the radiated case, the output of the channel emulator is connected to two antenna probes which will connect wirelessly to the DUT [18]. In the radiated case, the effect of the wireless channel is removed by applying the inverse of the channel transfer matrix to the output signal. In the radiated two-stage case, the self-interference from the DUT is included in the measurements, whereas in the conducted measurements they are not.

Reverberation Chamber (RC)

The Reverberation Chamber (RC) has been traditionally used for EMC testing. It consists of a metal cavity that supports many modes at the operating frequency [19]. The chamber contains metal plates that are moved inside the chamber to excite different modes. These plates are called mode stirrers, see Fig. 2.4. By placing the DUT on a turntable and changing the polarization by switching between different chamber antennas, more independent samples can be collected, and higher accuracy can be achieved [20]. The chamber can emulate a RIMP environment, which will be described more in detail in Section 2.2.1. Statistically, the emulated environment can be described as a multipath Rayleigh fading environment. It means that the amplitude variation of the received signals by the DUT follow a Rayleigh distribution, while the phase is uniformly distributed [21].

The first step to perform a measurement is to do a calibration. At this step, the

average power transfer function of the chamber, which is proportional to the radiation efficiencies of the transmitting and receiving antennas, is measured [22]. Measurements are then performed by connecting a communication tester to the chamber antenna in the RC. A metal shield in front of the chamber antenna is placed to makes sure that no LOS component is present. No channel emulator is needed if a regular Rayleigh fading environment is desired. However, a channel emulator can be used if additional variations, e.g., in Doppler and delay spread are wanted. There exist no specific test zone inside the chamber, as long as the DUT is placed at least $0.5\,\lambda$ away from any metal wall/plate.

2.2 Real-world Hypothesis

There is no easy way to evaluate the performance of different user devices in all possible, or even in most typical, environments. Ideally, it would be desirable to make sure that the device works well in all real-world environments in which it will be used in, but this is not feasible. However, in practice, typical channel models are used to emulate different real-world scenarios. A different idea is presented in [2], where a hypothesis is stated. It is formulated as follows *"If a wireless device is tested with good performance in both pure-LOS and RIMP environments, it will also perform well in real-life environments and situations, in a statistical sense"*. While this hypothesis is yet to be proven, it provides an appealing and practical framework within which many devices could be evaluated in a cost and time efficient way. The two edge environments, RIMP and Random-LOS are presented more in detail in the following sections and in Fig. 2.5.

2.2.1 Rich Isotropic Multipath (RIMP)

The Rich Isotropic Multipath (RIMP) environment is an ideal fading environment, that does not exist in reality, but that has been proven to be very useful [19]. The first word, Rich, refers to that there are many incoming waves simultaneously. Isotropic refers to that the Angle of Arrival (AoA) of the incoming waves are uniformly distributed over the unit sphere, which means that the orientation of the DUT will not matter. The last word multipath refers to that the waves have taken multiple paths to the receiver. The RIMP environment can be emulated in a reverberation chamber.

Real multipath environments are seldom isotropic like assumed in RIMP; however, if we consider a larger period of time and a number of mobile phone users, then the environment will be approximately so [23]. The reason is that mobile devices can be used in different orientations, e.g., in talk mode and surf-mode, and they are located in different locations in respect to a base station.

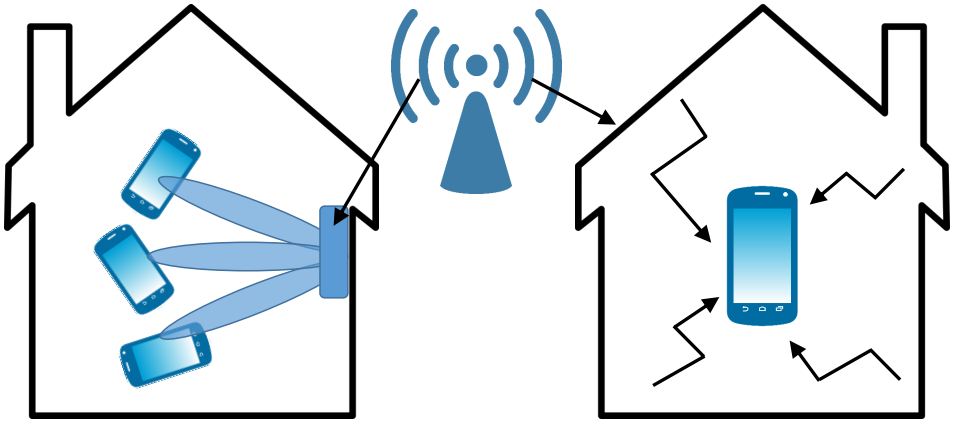

	Random Line-of-Sight	Real world	Rich Isotropic Multipath
Waves	One dominating	?	Many simultaneously
Angle of Arrival	Random	?	Uniform distribution
Polarization	Random	?	Balance
Measurement method	Anechoic Chamber	Real-world tests	Reverberation Chamber

Figure 2.5: Comparison between Random-LOS and RIMP. The Random-LOS case is represented by a micro base station using massive MIMO and randomly oriented users. The RIMP case is represented by an indoor environment with a lot of scatterers and no LOS to the base station.

2.2.2 Random Line-of-Sight (Random-LOS)

The Random Line-of-Sight (Random-LOS) environment consists of a dominating incoming wave, which most of the time is a LOS contribution, but it can also be a strong diffracted or scattered wave [24]. The difference with the traditional LOS environment is that at least one of either the transmitter or receiver is randomly oriented. Usually it is the user device that is randomly oriented, since the base station normally is placed in a fix position [25]. By introducing an ensemble of users over time, the statistics of the DUT orientation will become increasingly random, and thereby the randomness in the LOS component will increase.

The randomness in Random-LOS refers both to random AoA and random polarization. When a DUT is randomly oriented in a 3D environment, both the polarization (considering linear polarization) and the AoA of the incoming wave will change relative to the DUT. Different user devices will experience either a 2D or a 3D Random-LOS, see Fig. 2.6. For example a small handset (i.e., a mobile phone or tablet) can be oriented in any direction in space, since people are using them in talk-mode, surf-mode, etc., see Fig. 2.7. Vehicles, on the other hand, will only be oriented randomly in the horizontal plane with some slight elevation angles. This corresponds to a 2D random AoA and one dominating polarization.

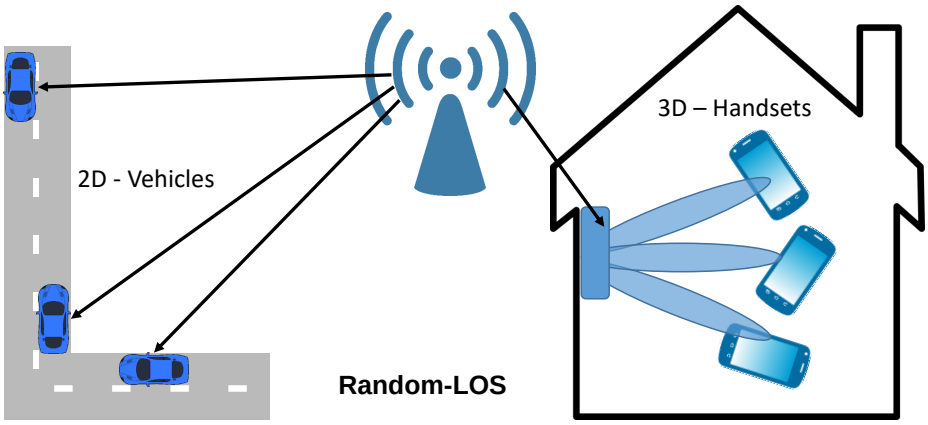

Figure 2.6: Realization of 2D and 3D Random-LOS. The 2D Random-LOS case is applicable for vehicles, whereas the 3D Random-LOS is more useful for mobile handsets.

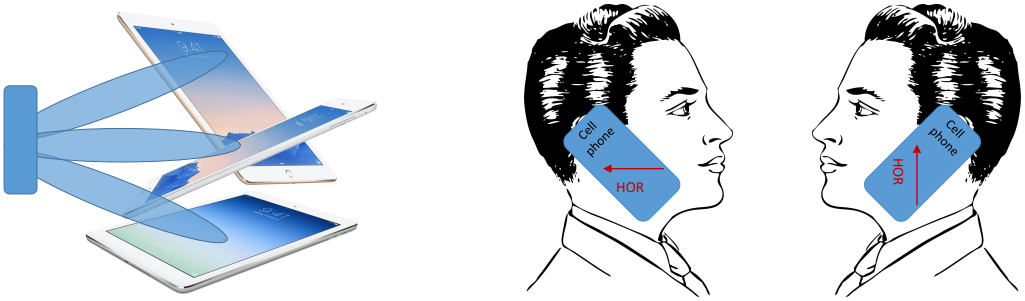

(a) (b)

Figure 2.7: Random AoA and random polarization due to the user behaviour.

Random-LOS Measurement Setup for Vehicles

An idea for realizing a Random-LOS test environment for testing the wireless communication performance of vehicles was presented in [26]. The Random-LOS is a relevant environment for vehicles, since vehicles often are used on highways and in rural areas where there is often a LOS component to the base station. To emulate a base station in Random-LOS, it is needed to perform measurements emulating the far-field region of the base station. By generating a plane wave, the far-field can be emulated. A plane wave can be realized by using for example a planar array [8,27,28]. In [29], simulations are shown for a planar array that can be used for a Random-LOS testing. However, the solution in [29] becomes too complicated and expensive to manufacture. Hence, a reflector with a linear array feed, similar to a compact range, is presented in [30,31].

The reflector solution for the chamber antenna is shown in Fig. 2.8. The feed of the reflector consists of a linear array feed of dual-polarized antenna elements. In [31], dual-polarized bowtie antennas are used as antenna elements [32]. The an-

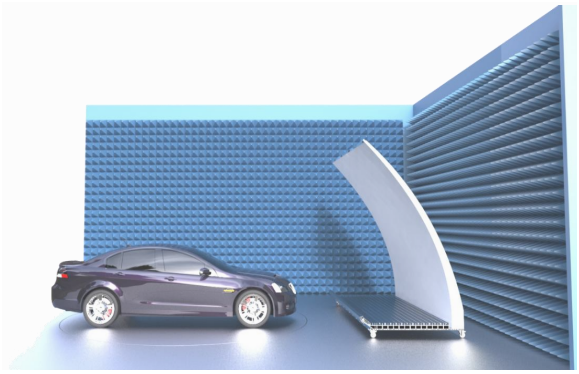

Figure 2.8: Sketch of the final Random-LOS measurement setup solution with a reflector and a linear array feed for creating a plane wave illumination of the car.

tenna elements in the array are combined using a beamforming network, where the combination is done separately for each polarization. This results in two ports on the chamber antenna, i.e., one for each polarization. By connecting a communication tester to the ports, a base station in far-away LOS can be realized. When the vehicle is rotated on a turntable, the performance can be evaluated for different rotation angles or different AoAs. In this way, the 2D Random-LOS environment can be realized for testing the system performance of vehicular wireless communication.

The reflector solution is modular and can easily be made wider by extending the linear array feed and adding an extra piece to the reflector. The suggested reflector in [31] has a height of 3 m, a width of 4 m and a depth of 1.5 m.

2.3 Wireless Communication

With the development of the wireless communication, came also the use of several antennas on both the transmitter (TX) and the receiver (RX) sides, see Fig. 2.9. This can be divided into Single-Input Single-Output (SISO), Single-Input Multiple-Output (SIMO), Multiple-Input Single-Output (MISO) and Multiple-Input and Multiple-Output (MIMO) scenarios [33]. Input refers to the TX side and output refers to the RX side and single means that only one antenna is used, whereas multiple means that several antennas have been used.

A MIMO system can be described by

$$\mathbf{y} = \mathbf{H}\mathbf{x} + \mathbf{n} \ , \tag{2.2}$$

where $\mathbf{y}$ is the output of the channel, $\mathbf{x}$ is the input, $\mathbf{H}$ is the channel matrix and $\mathbf{n}$ is the noise vector. It is possible to decompose the MIMO channel into independent parallel channels. More independent channels can be achieved in a more rich scattering environment than in a LOS environment [34]. However, the maximum number

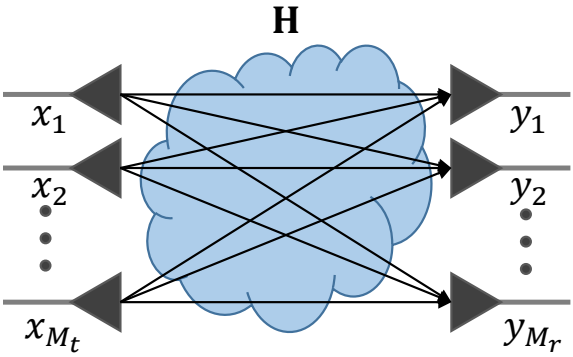

Figure 2.9: MIMO system.

of independent channels depends also on the number of transmit M_t and receive M_r antennas. The number of independent channels, R, is limited by $R \leq \min(M_t, M_r)$, and in general, on the rank of the channel matrix $\mathbf{H}$. Multiplexing, where different data is transmitted on every channel, can be used in a MIMO system to increase the capacity. In order to separate the signals, different schemes can be used, e.g., singular value decomposition and zero forcing (ZF). In this thesis, we have used ZF which relies on the pseudo-inverse of the channel matrix, to separate the signals at the receiver [35].

Instead of increasing the capacity, diversity can be used, where several copies of the same data is transmitted or received, which makes the system more stable and less vulnerable to fading dips. There exist different combining schemes to combine data at the receiver ports, e.g., selection combining (SC), equal-gain combining (EGC) and maximal-ratio combining (MRC) [33]. In this thesis, we have used MRC for receive diversity in several cases. In MRC, the received signals at all the ports are weighted and summed together to obtain the maximum signal to noise ratio. The weights are chosen proportionally to the signal to noise ratio at the ports.

2.3.1 The Threshold Receiver Model

In [3], the threshold receiver model is presented. It is a model for calculating the throughput data rate for wireless LTE devices. The model is based on the group error rate (GER), which contains the error rates that are used to measure the performance of receivers. It has been noted that in a static environment, the GER changes quickly from 100 % to 0 % at a certain threshold power, P_t. This can be written as

$$\mathrm{GER}_{\mathrm{ideal}}(P) = \begin{cases} 1, & \text{when } P < P_t \\ 0, & \text{when } P > P_t \end{cases} . \tag{2.3}$$

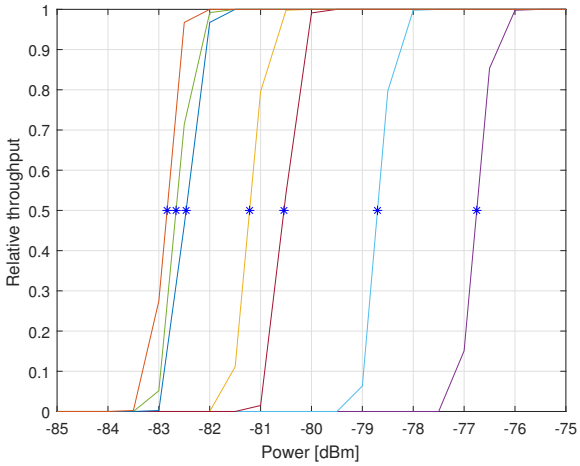

Figure 2.10: Threshold levels in a static environment.

The throughput TPUT, can then be straightforwardly expressed in terms of the maximum throughput $\mathrm{TPUT}_{\mathrm{max}}$ and the GER,

$$\mathrm{TPUT} = \mathrm{TPUT}_{\mathrm{max}} * (1 - \mathrm{GER}(P)) \ . \tag{2.4}$$

The maximum throughput depends on parameters such as the modulation and coding.

Fig. 2.10 shows the single threshold levels measured for different orientations of a DUT in a Random-LOS environment. It can be clearly seen that the data throughput abruptly changes from full to zero in a static environment. For different orientations, this change happens at different power levels, due to the non-isotropic radiation pattern of the DUT. These threshold values are what we are interested in measuring. Since the change is very steep, it is possible to represent the threshold by the power level at which it occurs, as shown with a star ($*$) in the figure. This is also referred as level of detection threshold. A measurement in a static Random-LOS environment behaves in the same way as a conducted measurement with respect to the appearance of the threshold. The corresponding theoretical thresholds would be a perfect step-like curve.

The average GER is expressed as a function of the average power level P_{av} as

$$\mathrm{GER}_{\mathrm{av}}(P_{\mathrm{av}}) = \int_0^{\infty} \mathrm{GER}_{\mathrm{static}}(P)\mathrm{PDF}(P/P_{\mathrm{av}})\mathrm{d}P \ , \tag{2.5}$$

where PDF is the Probability Density Function. This is valid for frequency flat fading, which means that the bandwidth is much smaller than the coherence bandwidth. Using Equation (2.3)-(2.5) we rewrite the average GER into

$$\mathrm{GER}_{\mathrm{av}}(P_{\mathrm{av}}) = \int_0^{P_t} \mathrm{PDF}(P/P_{\mathrm{av}})\mathrm{d}P = \mathrm{CDF}(P_t/P_{\mathrm{av}}) \ , \tag{2.6}$$

where CDF is the Cumulative Distribution Function. From this, we obtain the throughput as

$$\mathrm{TPUT} = \mathrm{TPUT}_{\max} * [1 - \mathrm{CDF}(P_t/P_{\mathrm{av}})] \ . \tag{2.7}$$

The probability of detecting a bitstream is thus related to the throughput threshold [25]. When the received power is above the threshold level, the received data will be of sufficient quality to detect and decode the received bitstream, whereas if the power is below the threshold, it will not be detected. By counting the number of times the received power level is above the threshold (the bitstream will be detected), and divide it with the total number of samples, you get the Probability of Detection (PoD). If the same modulation scheme and coding are used for all samples, the PoD becomes equal to the relative throughput

$$\mathrm{PoD}(P_{\mathrm{av}}) = \frac{\mathrm{TPUT}_{\mathrm{av}}(P_{\mathrm{av}})}{\mathrm{TPUT}_{\max}} = 1 - \mathrm{CDF}(P_t/P_{\mathrm{av}}) \ . \tag{2.8}$$

Chapter 3

Characterization of the Test Zone

In a Random-LOS environment, one wants to evaluate the performance of a wireless device in the far-field. This can be realized by creating a plane wave close to the chamber antenna. The final Random-LOS measurement setup for vehicular applications will use a reflector with a linear array feed to realize the plane wave, see Fig. 2.8. Another way to generate a plane wave is to use a planar array [8,28,36]. In this chapter we consider three different types of chamber antennas, a single antenna element (SAE), a horizontal uniform linear array (ULA) and a uniform planar array (UPA). The three antennas are compared in terms of their capabilities of generating a field emulating a plane wave in the test zone. The comparison is made both by simulations and measurements performed in an AC at Chalmers.

The performance evaluation is done by looking at the power and phase spread, which are defined below:

- ***Power spread:*** The sample standard deviation σ_{dB} is computed in dB, by using [37],

$$\sigma_{\mathrm{dB}} = 5\log\left(\frac{1+\sigma}{1-\sigma}\right) , \tag{3.1}$$

  where σ is the standard deviation of the normalized power in linear units, i.e.,

$$\sigma = \sqrt{\mathrm{VAR}\left\{\frac{P}{\mathrm{MEAN}\{P\}}\right\}} , \tag{3.2}$$

  where $\mathrm{VAR}\{.\}$ and $\mathrm{MEAN}\{.\}$ are the sample variance and sample mean operations, respectively. P is the power and is defined as $P = |\sum E_z|^2$ for the simulations and by $P = |\sum S_{21}|^2$ for the measurements.

- ***Phase spread:*** The variation of the phase ϕ is evaluated as the maximum phase deviation from the mean

$$\Delta\phi_{\max} = \max|\phi - \mathrm{MEAN}\{\phi\}| . \tag{3.3}$$

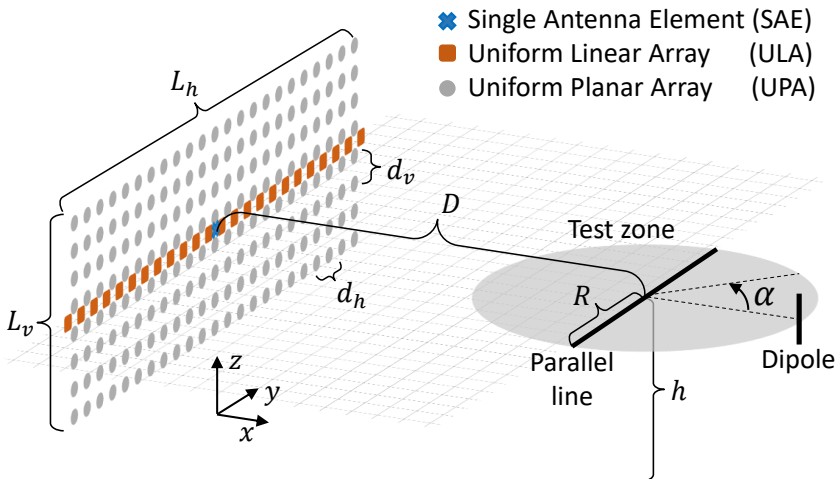

Figure 3.1: Setup for the three different chamber antenna test cases; the single antenna element (SAE), the horizontal uniform linear array (ULA) and the uniform planar array (UPA).

The phase ϕ is defined as $\phi = \arg\{\sum E_z\}$ for the simulations and by $\phi = \arg\{\sum S_{21}\}$ for the measurements, where $\arg\{.\}$ denotes the operation of taking the argument of a complex number.

In this chapter we will also study how the performance differs for different chamber antennas in the presence of a ground reflection, for example as in a semi-anechoic chamber. This is studied both by simulations and measurements. The measurements are done in a semi-anechoic chamber with a shark-fin antenna mounted on the roof of a car. The frequency response is measured for two different chamber antennas, a single antenna element and a vertical 8-element linear array. This chapter is based on paper A and B.

3.1 Random-LOS Measurement Uncertainty

It is important to evaluate the measurement uncertainty in the Random-LOS measurement setup to ensure that measurements can be performed with an acceptable accuracy. This section, which is based on paper A, is a continuation of work done in [29, 30]. It shows the measurement accuracy for three different types of movement patterns in a test zone in front of the chamber antenna. The investigations are performed at $f = 2.7\,\text{GHz}$ and done along a parallel line, along the rim of a circle and the area within a circular test zone, see Fig. 3.1. We are not interested in the absolute values of the field, but rather the relative variation of the power $P_{\text{norm}} = P/\text{MEAN}\{P\}$ and phase $\phi_{\text{norm}} = \phi/\text{MEAN}\{\phi\}$ within these areas, as indicated by Equation (3.1)-(3.3). This means that all results in the figures are presented normalized to their mean values.

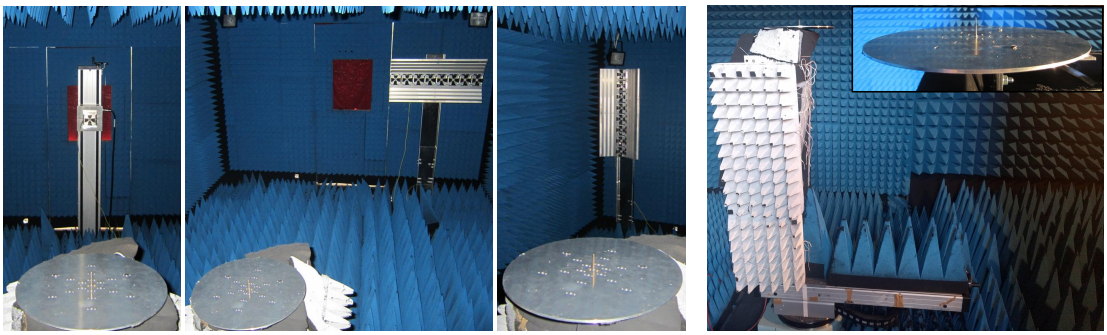

(a) (b)

Figure 3.2: Measurement setup in the anechoic chamber at Chalmers University of Technology. (a) Measurement setup for the three different chamber antennas; single bowtie (SAE), horizontal ULA (partly) and UPA (partly). (b) The monopole with its ground plane mounted on the turntable.

Simulations using a Method of Moments (MoM) software and measurements in an AC at Chalmers were performed for three different types of chamber antennas. The chamber antennas are defined by the number of antenna elements $N = N_v \times N_h$, where N_v and N_h are the elements in the vertical and horizontal directions, respectively. The three types consist of a single antenna element (SAE), a 1×24 horizontal uniform linear array (ULA) and a 8×23 uniform planar array (UPA). Both the ULA and UPA cases were realized in the measurements by using a smaller 8-element ULA, to virtually create larger arrays. The smaller array was placed in different adjacent positions and by combining the contributions from all the positions a virtual larger array can be reconstructed, similar to a synthetic-aperture radar. As mentioned in Section 2.2.2, a distribution network is used, one for each polarization, to combine the contributions from all the antenna elements. In all the measurements, a monopole, mounted on a circular ground plane with a radius of 0.28 m, was used to sample the field in front of the chamber antennas, see Fig. 3.2.

In the simulations the same scenario is reproduced as in the measurements, by using reciprocity. Instead of measuring the field in front of the chamber antenna, a transmitting z-oriented dipole is moved in a grid in front of the simulated chamber antenna. The z-component of the E-field from the dipole is sampled, at the same positions as the antenna elements in the chamber antenna array. By combining the complex E-field values from different sample positions it is possible to reconstruct the E-field from the virtual chamber antenna.

In Fig. 3.3, simulation results for the three different chamber antennas are presented. The power and phase variations for an area of size 5 m $\times$ 5 m in front of the chamber antennas are shown.

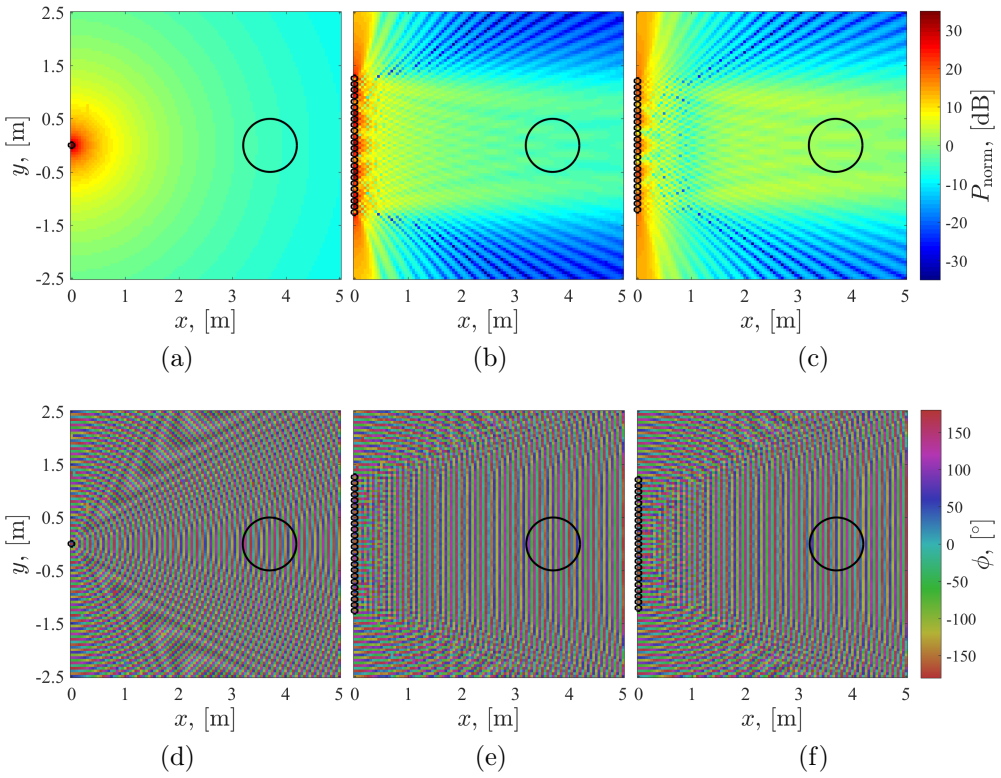

Figure 3.3: Simulated power variation in an area of 5 m × 5 m in front of three different antennas placed in a free-space environment. The columns, from left to right, correspond to the SAE ($N = 1$), the ULA ($N = 1 \times 24$) and the UPA ($N = 8 \times 24$), see Fig. 3.1. The first row shows the normalized power variation and the second row shows the phase variation.

Table 3.1: Uncertainty shown as power spread, σ_{dB} and phase spread, $\Delta\phi_{\max}$ along a parallel line with a length of $2R = 1$ m, corresponding to the results in Fig. 3.4.

		SAE	ULA	UPA
σ_{dB}, [dB]	Sim	0.02	0.60	1.02
	Meas	0.63	1.00	0.83
$\Delta\phi_{\max}$, [°]	Sim	73	10	13
	Meas	95	26	23

3.1.1 *Line* Uncertainty

To evaluate the plane wave behaviour it is important to study the the power and the phase variation along a parallel line in front of the chamber antenna, see Fig. 3.1. An ideal plane wave will in fact have no power and phase variations along this line. Simulated data is shown together with measured data in Fig. 3.4. The power and phase spread along this parallel line are summarized in Table 3.1.

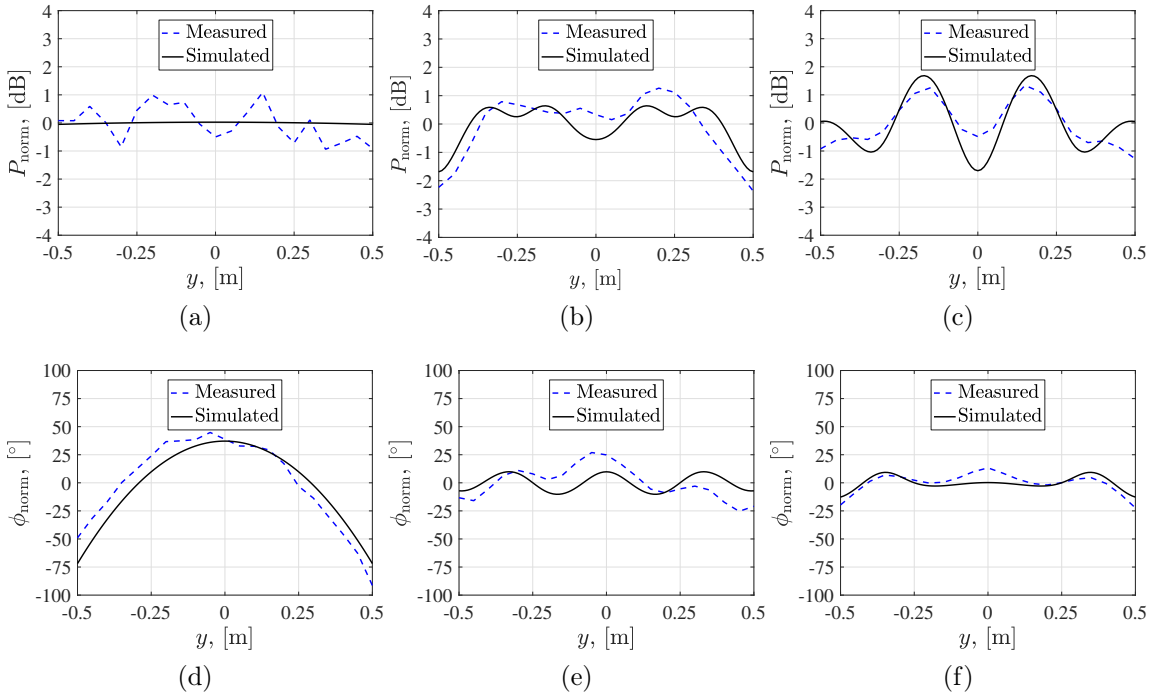

Figure 3.4: Power and phase comparisons between theoretical and measured data along a parallel line in front of the chamber antenna, i.e., *line* uncertainty, see Fig. 3.1. The columns, from left to right, correspond to the SAE ($N = 1$), the ULA ($N = 1 \times 24$) and the UPA ($N = 8 \times 24$).

Table 3.2: Power spread, σ_{dB}, for the different measurement and simulation cases. The variation along the rim and within the circular test zone are both shown for a radius of 0.5 m.

			SAE	ULA	UPA
σ_{dB}, [dB]	Circle	Sim	0.86	1.41	0.77
		Meas	1.19	2.07	1.04
	Test zone	Sim	0.60	0.85	0.86
		Meas	0.79	1.09	0.77

3.1.2 *Circle* Uncertainty

When the position of the antenna on the car is known and the car is rotated on the turntable, it is important to consider how the amplitude can vary along the rim of the test zone. How this vary for a rotation radius of 0.5 m can be seen in Fig. 3.5 for the three different chamber antennas. Good agreement is seen between the simulated and measured data. This data is also summarized in Table 3.2.

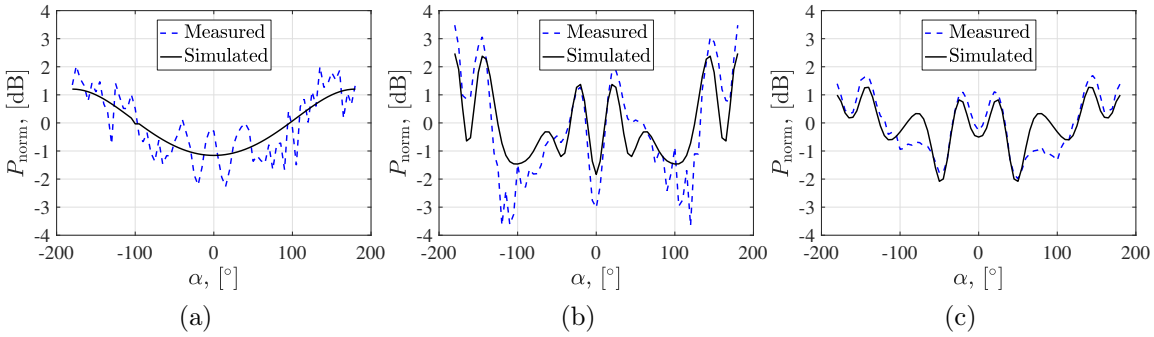

Figure 3.5: Power comparisons between theoretical and measured data for a rotation with 0.5 m radius. The columns, from left to right, correspond to the SAE ($N = 1$), the ULA ($N = 1 \times 24$) and the UPA ($N = 8 \times 24$).

3.1.3 Test Zone Uncertainty

In order to somewhat relax the need to determine the exact location of antennas within the test zone, or if multiple antennas on the car are tested at the same time, it is important to ensure that, as long as the antennas under test are within the predefined test zone, the standard deviation of the power spread will not exceed a certain value. For different test zone sizes, different corresponding standard deviation values can be calculated. In Fig. 3.6, simulated and measured power variations in a test zone with radius 0.5 m are shown. The power and phase spread is shown in Table 3.2. The same data presented in Fig. 3.6 is used to create Fig. 3.7(a), where the power spread is shown as a function of test zone radius.

3.2 Ground Reflection Suppression

The semi-anechoic chambers are a convenient option for the Random-LOS measurement set-ups, especially for vehicular applications. In these chamber, the ceiling and the walls are covered with RF absorbing materials, while the floor is made of metal. In simulations, this could be realized by a perfect electric conductor (PEC) ground plane. For an ideal Random-LOS environment, ground reflections are not desired, since their contribution will vary depending on the distance to the test object [38]. This undesired effect on the reference signal variation in the test zone therefore needs to be removed. Free-space simulations from Section 3.1 were compared to the same three cases when a PEC was used as a ground plane. This is presented in Fig. 3.7(b). It can be seen that the planar array performs the same, independent of the presence of the ground plane. On the other hand, when the ground plane is added, a significant degradation is seen in the permanence of the other cases.

To further investigate the ground reflection, measurements were done in a semi-anechoic chamber, where the frequency response was measured for a roof mounted

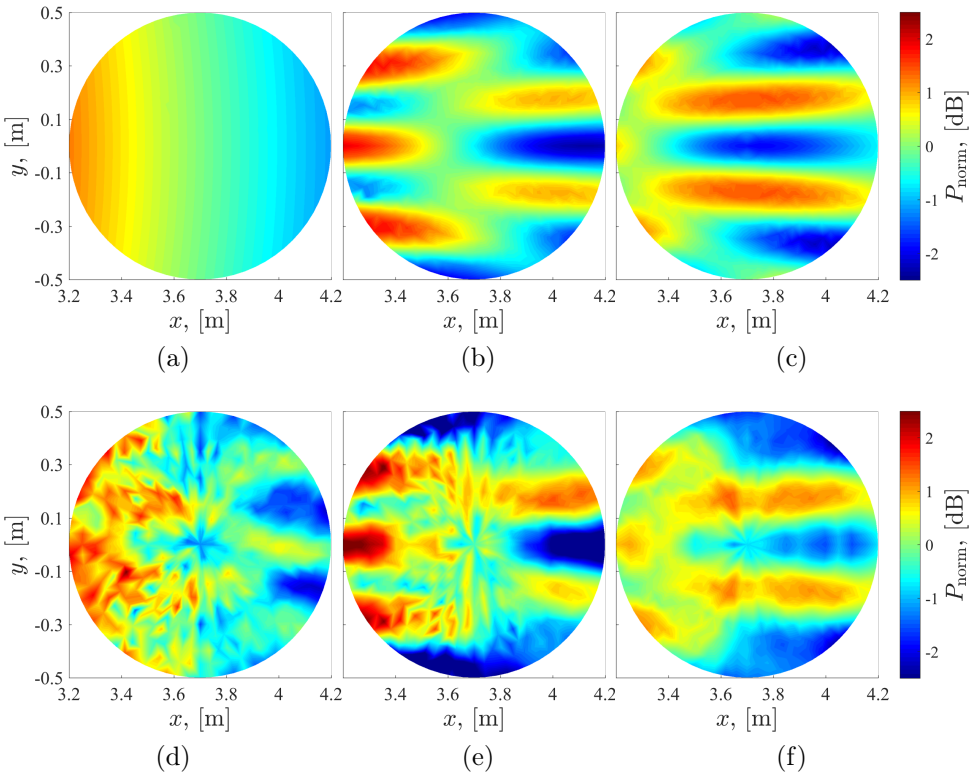

Figure 3.6: Power variations for the three investigated cases, both simulations and measurements. The plotted area is shown as the black circle in Fig. 3.3. The columns, from left to right, correspond to the SAE ($N = 1$), the ULA ($N = 1 \times 24$) and the UPA ($N = 8 \times 24$). The first row shows the simulated and normalized power variation and the second row shows the measured normalized power variation.

shark-fin antenna on a Volvo XC90, see Fig. 3.8. Two sets of measurements are performed with the two antennas used as chamber antenna, i.e., see Section 3.1. The first one is the single bowtie antenna, and the second is the 8-element bowtie array placed in a vertical position ($N = 8 \times 1$), i.e., one of the positions used for the virtual planar array. The frequency response as a function of rotation angle is shown in Fig. 3.9.

It can be seen that with an extension of the array in the vertical direction, i.e., the z-axis, one can suppress the contribution from the ground reflection and obtain a more pure Random-LOS environment. The constructive and destructive interference due to the ground reflection can be seen for the single chamber antenna cases for the rotation angles around 180 °. This corresponds to the angles where the back of the car is facing the chamber antenna, i.e., the shark-fin antenna is more directly exposed to the ground reflection. The array figures in Fig. 3.9 have an overall higher power, which is due to the array gain.

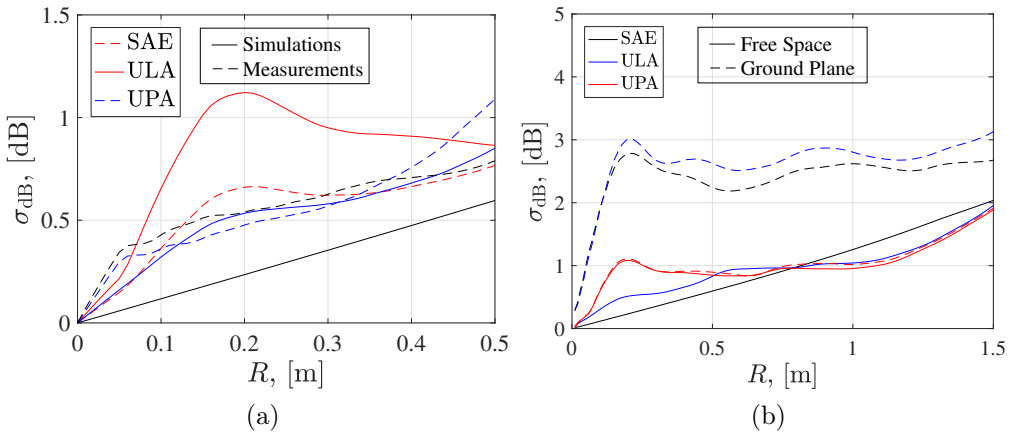

Figure 3.7: Standard deviation within the whole test zone as a function of the test zone radius. Results are shown for both single, horizontal and planar array antenna. (a) The standard deviation for the simulated data and the corresponding measured data. (b) Standard deviation for the simulated free-space and PEC ground plane case.

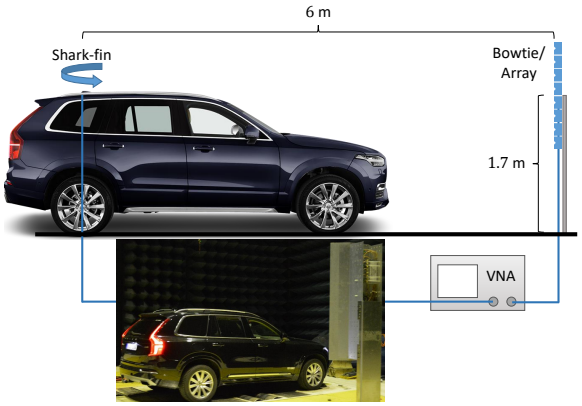

Figure 3.8: The Random-LOS measurement setup with a vertical bowtie array as a chamber antenna and roof mounted shark-fin antenna, on a Volvo XC90, as antenna under test. The front of the car facing the chamber antenna, as shown in the figure, corresponds to the rotation angle $\alpha = 0\,^{\circ}$.

3.3 Summary and Conclusions

The UPA is the chamber antenna that has the best over-all performance, in terms of power spread and phase spread for both a free-space environment and an environment with a PEC as a ground plane, i.e., a semi-anechoic chamber. The measured and simulated data match well and a standard deviation of less than 0.9 dB can be achieved for the power within a test zone of radius $R = 0.5$ m for the UPA (8×23 elements). The results indicate that the desired Random-LOS reference environment can be generated in both full- and semi-anechoic environments.

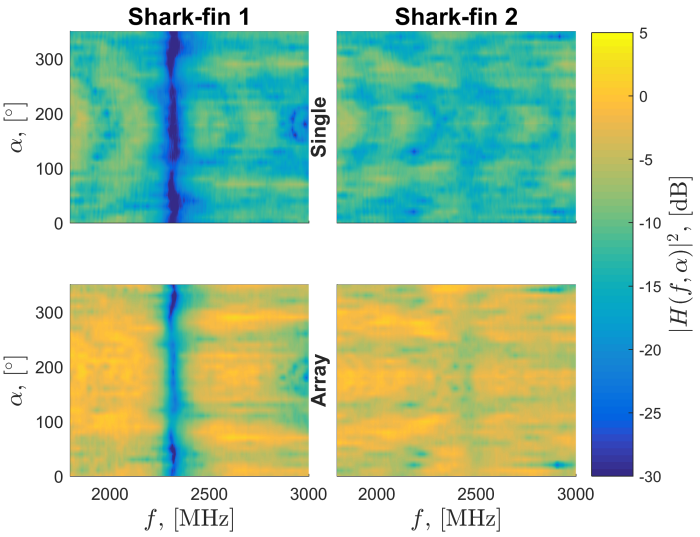

Figure 3.9: The frequency response plotted as a function of frequency and rotation angle, α.

Chapter 4

Throughput Measurements in the Random-LOS Environment

There exists the need to evaluate the communication system performance of connected vehicles in a systematic way. However, currently, there are no standardized solutions to fulfil this. Moreover, the available proposed ideas come from scaled up versions, already used for mobile phone testing. This chapter shows how the Random-LOS measurement setup could instead be used to test the communication system performance of connected vehicles. To show the main ideas behind the concept and to find out how testing can be performed practically, initial tests have been performed with a simplified measurement setup.

In order to understand the Random-LOS environment, it is important to look into and study the different parts in detail. In this chapter, both randomness in Angle of Arrival (AoA) and polarization are studied (see Section 2.2.2). The testing is done in terms of OTA data throughput for LTE. This chapter is based on papers C, D and E.

4.1 Random Polarization

The random polarization effect in a pure Random-LOS environment was studied in paper E. Two dual-polarized antennas were used, a quadridge horn antenna (ETS Lindgren Open Boundary Quadridge Horn, Model 3164-05) and a dual-polarized 2-port bowtie antenna [39]. By connecting one antenna to a base station simulator and the other to an LTE modem it is possible to perform active testing in a polarization Random-LOS environment. The polarization Random-LOS environment is realized by placing both antennas in an anechoic chamber facing each other. The polarization randomness is then created by rotating the chamber antenna, i.e., the quadridge horn, around the z-axis, see Fig. 4.1.

By sweeping the power and measuring the data throughput for a range of rotation

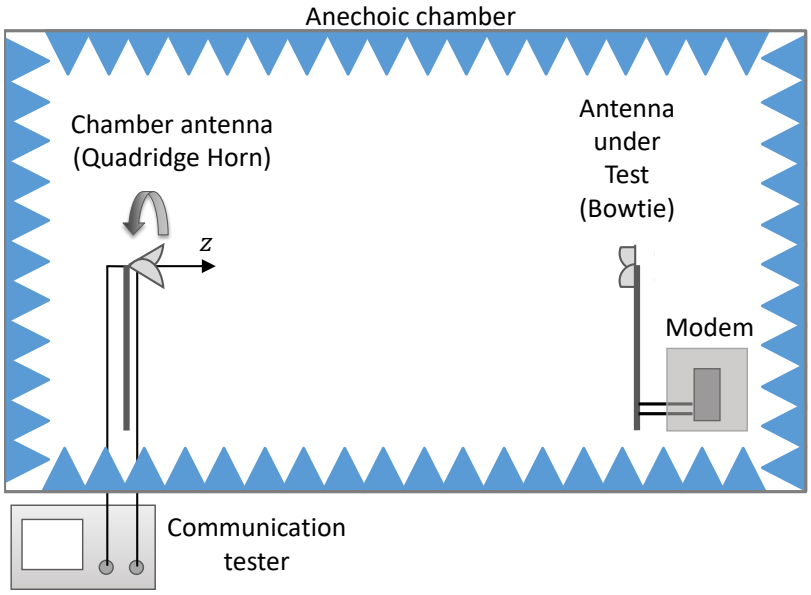

Figure 4.1: Polarization Random-LOS test setup.

angles it is possible to see how the active performance varies when there is a polarization mismatch. In paper E, the impact of the amplitude imbalance of the two orthogonal polarizations is shown to affect the measured throughput performance. All the measurements were performed at $f = 2.655\,\text{GHz}$.

The results for SISO, SIMO and MIMO are shown in Fig. 4.2. The markers represent the level of detection threshold, see Section 2.3.1. Different markers are used to represent three different measurement sequences. The theoretical SISO curve corresponds to a polarization mismatch with a $\cos^2\phi$-dependency. The theoretical curves for the SIMO case are based on maximal ratio combining (MRC) receiver. In this receive diversity mode, with a dual-polarized antenna with the same amplitude on both ports, the signal can be detected equally well, regardless of the transmit polarization [34]. However, if there is an amplitude imbalance, a degradation in performance will be seen for some angles. This is visible in Fig. 4.2(e)-(f) when an artificial 3 dB amplitude imbalance is introduced with an attenuator.

The 2×2 MIMO case will perform in the same way as SIMO when the ports have equal amplitude and orthogonal polarizations, except that in theory, it will result in a 3 dB degradation since the transmit power is divided on the two bitstreams, see Fig. 4.2(g). An added amplitude imbalance of 3 dB can be seen as a 75 % average degradation of the performance, which corresponds to a degradation of 1.25 dB. The MIMO measurements with a 3 dB amplitude imbalance, Fig. 4.2(h)-(i), thus has a degradation of $0.7\,\text{dB} \pm 0.8\,\text{dB}$ compared to the amplitude balanced MIMO case. The measurement uncertainties seen in the figures may partly be due to the chamber itself which is not well enough shielded for active measurements. However, it is still

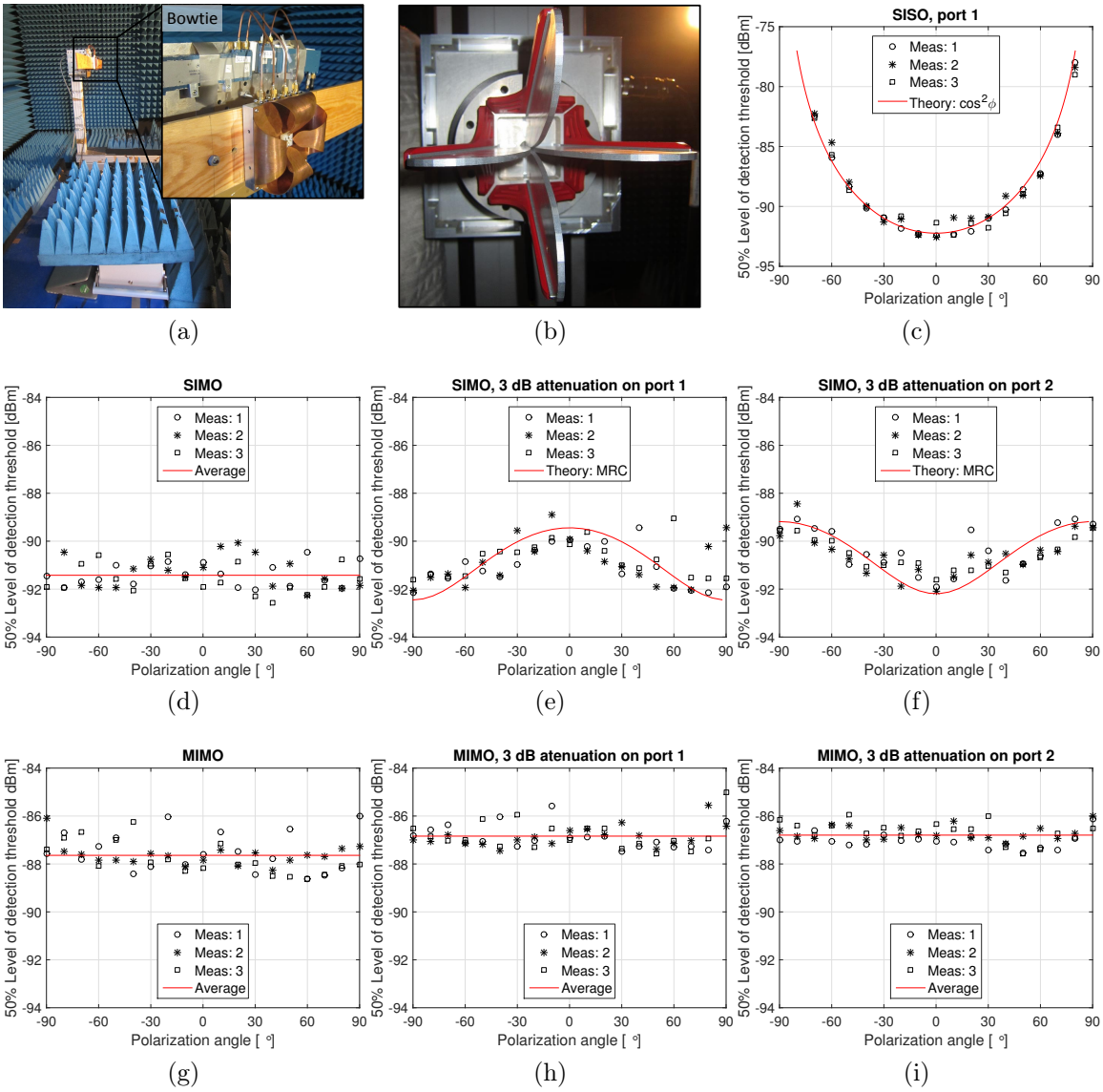

Figure 4.2: Polarization-Random-LOS measurements. (a) shows the measurement setup in the AC together with the bowtie antenna and (b) shows the quadridge horn antenna, corresponding to the antennas in Fig. 4.1. In (c) - (i) are the SISO, SIMO and MIMO measurement results are shown.

possible to see that the measurement results follow the theoretical values.

4.2 Random AoA

The random AoA was investigated for a simplified Random-LOS measurement setup. The simplified setup consists of a single dual-polarized chamber antenna and the

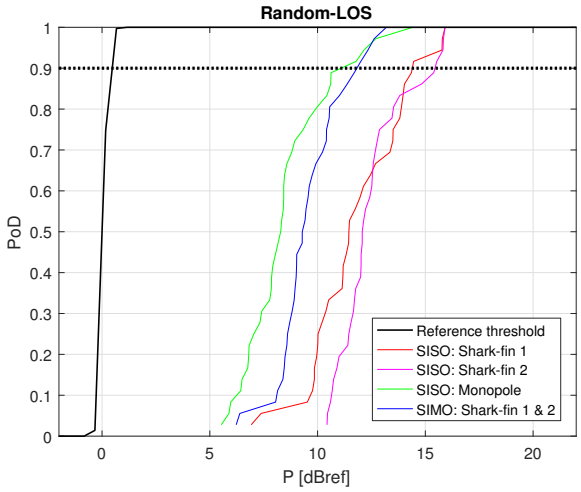

Figure 4.3: PoD in a Random-LOS environment shown for a two port LTE shark-fin antenna and a monopole mounted on the roof of a Volvo XC90.

quadridge horn antenna used in Section 4.1. The simplified measurement setup was used to test the general concept and evaluate how well measurements can be performed. This section is based on paper C and D.

Measurements in a semi anechoic chamber were performed at $f = 2.655\,\text{GHz}$ for a two-port LTE shark-fin antenna and a monopole mounted on the roof of a Volvo XC90. Additional measurements in a fully-anechoic chamber were performed on the same shark-fin antenna mounted on a square groundplane. The measurement results for the two cases can be seen in Fig. 4.3 and 4.4(a). The PoD curves were obtained by taking the CCDF of the level of detection threshold for the throughput curves, see Section 2.3.1. The measurements are all shown relative to a reference threshold, which in this case corresponds to the threshold of the reference bowtie antenna with a realized gain of 3 dBi. For this reason the power is shown in terms of dBref, i.e., dB relative to the reference threshold.

The difference in steepness between the results could be explained by a larger variation in the radiation pattern, expected when including the car in the measurements, which will result into a less steep PoD curve. The reason the SISO monopole performs the best can be explained by the antenna efficiency, which is expected to be higher than for the shark-fin. In fact the monopole is more narrowband, while the shark-fin antenna is designed for a wider bandwidth, at the expense of lower efficiency.

The throughput measurement results in the fully-anechoic chamber were complemented with theoretical curves. The theoretical curves are based on the radiation pattern of the shark-fin in the same measurement setup as for the active measurements. It is possible to compute the CDFs of the received signal from the radiation patterns of the AUT, by assuming uniformly distributed incident plane waves on the

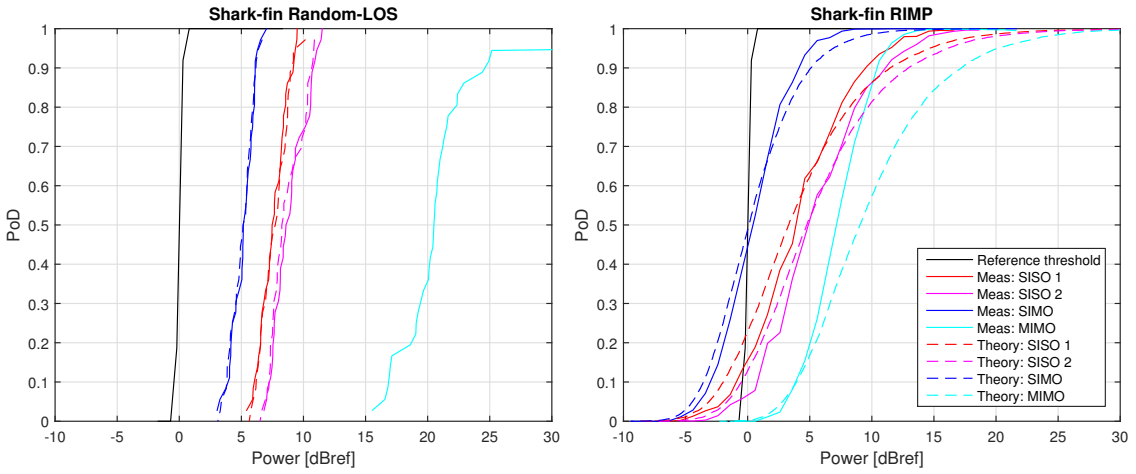

(a) (b)

Figure 4.4: Measured and theoretical PoD curves for the shark-fin antenna in the two edge environments. (a) Random-LOS measurements. The reference threshold corresponds to the threshold of the reference bowtie antenna, with a realized gain of 3 dBi [40]. (b) RIMP measurements. The reference threshold corresponds to the conducted reference threshold of the LTE dongle.

AUT. From the CDF, the PoD can be calculated, see Equation (2.8). The PoDs were then shifted according to the difference in the realized gain between the directive bowtie antenna and the omnidirectional shark-fin antenna. The SIMO curve was obtained by applying the Maximal Ratio Combining (MRC) algorithm to the radiation patterns of the two shark-fin antenna elements.

4.3 Complementary RIMP Measurements

Complementary measurements in a RIMP environment, realized in a RC, were performed for the shark-fin antenna mounted on a ground plane. It is interesting to see how the two edge environments from the real-world hypothesis, see Section 2.2, complement each other. This section is based on paper D.

The complementary RIMP results are presented in Fig. 4.4(b). The theoretical RIMP curves were computed using the threshold receiver model, Section 2.3.1, assuming a MRC receiver according to [41] for the SIMO curve and Zero Forcing (ZF) according to [42] for the MIMO curve.

By comparing the RIMP and the Random-LOS results in Fig. 4.4, it can be seen that the main difference is the general shape of the curves and the MIMO performance. It is hard to obtain MIMO performance in a LOS environment, since it is difficult to provide multiple independent channels in a small volume using only one polarization, see Section 2.3 [34]. To get MIMO performance in a LOS environment

one need to use two orthogonal polarizations as MIMO channels. The shark-fin antenna used in the measurements is single-polarized and the MIMO curve that is visible in the Random-LOS plot therefore shows the cross-polarization level of the antenna. The MIMO curves in the two figures have, in reality, higher throughput compared to the SISO and SIMO curves. However, this is not shown in the figure, since the curves are normalized to their maximum throughput.

4.4 Summary and Conclusions

Active measurements with the Random-LOS measurement setup can conveniently be performed. Expected performance was achieved both for random polarization and random AoA, both with antennas mounted on vehicles and on ground planes. Even with the simplified Random-LOS measurement setup, reasonable results can be obtained and the wireless communication performance of vehicles can be evaluated. The simplified setup shows promising results for future developments.

Chapter 5

Contribution and Future Work

The contributions are presented in this chapter as a summary of the appended papers, which can be found in Part II. At the end of this chapter, the future work directions are presented.

Paper A: Measurements and Simulations for Validation of the Random-LOS Measurement Accuracy for Vehicular Applications

Three different types of chamber antennas are evaluated in simplified Random-LOS measurement setups, a single antenna element, a 24 element horizontal uniform linear array and an 8×23 element uniform planar array. The evaluation is performed at $f = 2.7\,\mathrm{GHz}$ in terms of power and phase variation of the field in different test zones in front of the chamber antenna. Simulations are performed with a method of moments software and are compared to measurements. The larger arrays are emulated by using a technique similar to a synthetic aperture radar, i.e., the performance of a virtual array antenna is measured. It was found that with the 8×23 uniform planar array it is possible to obtain a standard deviation of less than $0.9\,\mathrm{dB}$ in power within a test zone with radius $0.5\,\mathrm{m}$.

Paper B: Evaluation of a Simplified Random-LOS Measurement Setup for Characterizing Antennas on Cars

The undesired ground reflection effect is evaluated on two different simplified Random-LOS measurement setups, one with a single antenna and the other with a vertical linear array as chamber antenna. The passive measurements were performed with a shark-fin antenna mounted on the roof of a car. The evaluation was focused on the dynamic range and delay spread of the received signal. The analysis considered each of the two antenna elements of the characterized shark-fin antenna. The analysis

shows that the ground reflection can be effectively removed by using an array antenna. A much better reference environment can then be achieved for Random-LOS OTA testing.

Paper C: Initial Measured OTA Throughput of 4G LTE Communication to Cars with Roof-Mounted Antennas in 2D Random-LOS

The active LTE throughput performances of different antennas mounted on a car are evaluated in a simplified 2D Random-LOS measurement setup. A roof-mounted shark-fin antenna with two antenna ports is measured for each port individually for SISO performance. The receive diversity (SIMO) of the 2-port antenna system was also evaluated. As reference, the performance of a roof-mounted monopole antenna was also measured. The evaluation is done in terms of the detection threshold and the probability of detection. The best antenna at 2.655 GHz was found to be the roof-mounted monopole antenna, which had the highest total radiation efficiency at the current frequency. Hence, the proposed Random-LOS OTA testing method was able to discern the performance of different antennas.

Paper D: Measured Probabilities of Detection for 1- and 2 Bitstreams of 2-port Car-roof Antenna in RIMP and Random-LOS

The same shark-fin antenna as in Paper C, but now mounted on a small square ground plane, is evaluated in both a RIMP and a simplified 2D Random-LOS environment. The LTE data throughput is measured and results are compared and presented as PoDs. Corresponding theoretical curves were calculated for the RIMP case by using the digital threshold receiver model together with maximal ratio combining and zero forcing receiver. Theoretical Random-LOS curves were obtained by measuring the radiation pattern and post processing the SIMO data using maximal ratio combining. As a result of the study, it was experimentally confirmed that in order to obtain two bitstreams in Random-LOS, dual-polarized antennas are required in compact shark-fin antennas.

Paper E: Measured LTE Throughput for SISO, SIMO and MIMO in Polarization-Random-LOS

In this paper, the random polarization is further investigated in a simplified Random-LOS environment. Two dual-polarized antennas are mounted facing each other. One of the antennas is rotated to study the polarization imbalance and its impact on data throughput. One of the antennas is connected to an LTE modem and the other to a

base station simulator. SISO, SIMO and MIMO LTE throughput measurements are presented as a function of the polarization mismatch. The behaviour is analyzed and compared with theoretical curves. The MIMO LTE was shown to be less sensitive to the polarization mismatch between the transmit and the receive antenna.

5.1 Future Work

The Random-LOS technology opens up for a huge number of opportunities in the era of the Internet of Things, when everything will be connected. The final design of the chamber antenna, i.e., the reflector with the linear array feed in Fig. 2.8, needs to be completed and manufactured. When the final prototype of the whole chamber antenna is manufactured it will need to undergo extensive verification. The performance needs to be measured to ensure that the simulated performance can be reached. This includes both active and passive measurements for a larger frequency range than has been studied until now. It would also be of interest to investigate the possibilities to extend the Random-LOS measurement solution to higher frequencies.

Moreover, the repeatability of the system needs to be investigated. Special attention will need to be given to the evaluation of the achievable accuracy within the test zone, for example by means of a thorough error budget analysis. The test zone should be extended not only to a circular plane in front of the antenna, but to a cylinder. It is also important to compare the performance with other methods in order to evaluate the performance more thoroughly.

It would also be interesting to further investigate the accuracy of the real-world hypothesis, by means of comparing measurements and simulations in real-life scenarios. Several challenges and research opportunities lies ahead to achieve affordable and practical antenna measurements for vehicular applications.

References

[1] 3GPP, "Verification of radiated multi-antenna reception performance of User Equipment (UE)," 3rd Generation Partnership Project, Technical Report 37.977 V14.5.0, Sep. 2017.

[2] P.-S. Kildal and J. Carlsson, "New approach to OTA testing: RIMP and pure-LOS reference environments and a hypothesis," in *2013 7th European Conference on Antennas and Propagation (EuCAP)*, Apr. 2013, pp. 315–318.

[3] P.-S. Kildal, A. Hussain, X. Chen, C. Orlenius, A. Skårbratt, J. Åsberg, T. Svensson, and T. Eriksson, "Threshold Receiver Model for Throughput of Wireless Devices With MIMO and Frequency Diversity Measured in Reverberation Chamber," *IEEE Antennas and Wireless Propagation Letters*, vol. 10, pp. 1201–1204, 2011.

[4] W. H. Kummer and E. S. Gillespie, "Antenna measurements-1978," *Proceedings of the IEEE*, vol. 66, no. 4, pp. 483–507, Apr. 1978.

[5] C. A. Balanis, *Antenna Theory*, 3rd ed. Hoboken, NJ, USA: Wiley-Interscience, 2005.

[6] I. IEEE, "IEEE Standard Test Procedures for Antennas," Tech. Rep. IEEE Std 149-1979, 1979.

[7] E. Joy, W. Leach, and G. Rodrigue, "Applications of probe-compensated near-field measurements," *IEEE Transactions on Antennas and Propagation*, vol. 26, no. 3, pp. 379–389, May 1978.

[8] J. Hansen, *Spherical NearField Antenna Measurements*, ser. Electromagnetic Waves Series. London, U.K.: Peter Peregrinus Ltd, 1988, no. 26.

[9] R. Johnson, H. Ecker, and R. Moore, "Compact range techniques and measurements," *IEEE Transactions on Antennas and Propagation*, vol. 17, no. 5, pp. 568–576, Sep. 1969.

References

[10] R. C. Johnson, H. A. Ecker, and J. S. Hollis, "Determination of far-field antenna patterns from near-field measurements," *Proceedings of the IEEE*, vol. 61, no. 12, pp. 1668–1694, Dec. 1973.

[11] C. Parini, *Theory and Practice of Modern Antenna Range Measurements*, ser. IET Electromagnetic Waves Series. London: The Institution of Engineering and Technology, Dec. 2014.

[12] 3GPP, "User Equipment (UE) / Mobile Station (MS) Over The Air (OTA) antenna performance; Conformance testing," 3rd Generation Partnership Project, Technical Specification 34.114 V12.2.0, Sep. 2016.

[13] P. Kyösti, T. Jämsä, and J.-P. Nuutinen, "Channel Modelling for Multiprobe Over-the-Air MIMO Testing," *International Journal of Antennas and Propagation*, vol. 2012, May 2012.

[14] W. Fan, F. Sun, J. Ø. Nielsen, X. Carreño, J. S. Ashta, M. B. Knudsen, and G. F. Pedersen, "Probe Selection in Multiprobe OTA Setups," *IEEE Transactions on Antennas and Propagation*, vol. 62, no. 4, pp. 2109–2120, Apr. 2014.

[15] M. G. Nilsson, P. Hallbjörner, N. Arabäck, B. Bergqvist, T. Abbas, and F. Tufvesson, "Measurement Uncertainty, Channel Simulation, and Disturbance Characterization of an Over-the-Air Multiprobe Setup for Cars at 5.9 GHz," *IEEE Transactions on Industrial Electronics*, vol. 62, no. 12, pp. 7859–7869, Dec. 2015.

[16] 3GPP, "User Equipment (UE) antenna test function definition for two-stage Multiple Input Multiple Output (MIMO) Over The Air (OTA) test method," 3rd Generation Partnership Project, Technical Report 36.978 V13.2.0, Jun. 2017.

[17] M. Rumney, H. Kong, Y. Jing, Z. Zhang, and P. Shen, "Recent advances in the radiated two-stage MIMO OTA test method and its value for antenna design optimization," in *2016 10th European Conference on Antennas and Propagation (EuCAP)*, Apr. 2016, pp. 1–5.

[18] W. Yu, Y. Qi, K. Liu, Y. Xu, and J. Fan, "Radiated Two-Stage Method for LTE MIMO User Equipment Performance Evaluation," *IEEE Transactions on Electromagnetic Compatibility*, vol. 56, no. 6, pp. 1691–1696, Dec. 2014.

[19] P.-S. Kildal, *Foundations of Antenna Engineering - A Unified Approach for Line-Of-Sight and Multipath*, 2015th ed. Kildal Antenn AB, May 2015, available at www.kildal.se.

[20] K. Rosengren, P.-S. Kildal, C. Carlsson, and J. Carlsson, "Characterization of antennas for mobile and wireless terminals in reverberation chambers: Improved accuracy by platform stirring," *Microwave and Optical Technology Letters*, vol. 30, no. 6, pp. 391–397, Sep. 2001.

[21] J. Kostas and B. Boverie, "Statistical model for a mode-stirred chamber," *IEEE Transactions on Electromagnetic Compatibility*, vol. 33, no. 4, pp. 366–370, Nov. 1991.

[22] D. Hill, M. Ma, A. Ondrejka, B. Riddle, M. Crawford, and R. Johnk, "Aperture excitation of electrically large, lossy cavities," *IEEE Transactions on Electromagnetic Compatibility*, vol. 36, no. 3, pp. 169–178, Aug. 1994.

[23] P. H. Lehne, A. A. Glazunov, and K. Karlsson, "Finding the distribution of users in a cell from smart phone based measurements," in *2016 International Symposium on Wireless Communication Systems (ISWCS)*, Sep. 2016, pp. 538–542.

[24] P.-S. Kildal, "Preparing for GBit/s Coverage in 5g: Massive MIMO, PMC Packaging by Gap Waveguides, OTA Testing in Random-LOS," in *2015 Loughborough Antennas & Propagation Conference*, Nov. 2015.

[25] P. Kildal, X. Chen, M. Gustafsson, and Z. Shen, "MIMO Characterization on System Level of 5g Microbase Stations Subject to Randomness in LOS," *IEEE Access*, vol. 2, pp. 1062–1075, 2014.

[26] P.-S. Kildal, A. A. Glazunov, J. Carlsson, and A. Majidzadeh, "Cost-effective measurement setups for testing wireless communication to vehicles in reverberation chambers and anechoic chambers," in *2014 Conference on Antenna Measurements Applications (CAMA)*, Nov. 2014, pp. 1–4.

[27] R. Haupt, "Generating a Plane Wave in the Near Field with a Planar Array Antenna," *Microwave Journal*, vol. Vol. 46, no. 9, pp. 152–166, 2003.

[28] D. A. Hill, "A Numerical Method for Near-Field Array Synthesis," *IEEE Transactions on Electromagnetic Compatibility*, vol. EMC-27, no. 4, pp. 201–211, Nov. 1985.

[29] A. A. Glazunov, A. Razavi, and P.-S. Kildal, "Simulations of a planar array arrangement for automotive Random-LOS OTA testing," in *2016 10th European Conference on Antennas and Propagation (EuCAP)*, Apr. 2016, pp. 1–5.

[30] A. Razavi, A. A. Glazunov, P.-S. Kildal, and R. Maaskant, "Array-fed cylindrical reflector antenna for automotive OTA tests in Random Line-Of-Sight," in *2016 10th European Conference on Antennas and Propagation (EuCAP)*, Apr. 2016, pp. 1–4.

References

[31] A. Razavi, "Characterization and Design Requirements for Antennas in the Near-field and the Random-LOS Propagation Environment," Doctoral thesis, Chalmers University of Technology, 2016.

[32] S. M. Moghaddam, A. A. Glasunov, and J. Yang, "Wideband Dual-Polarized Linear Array Antenna For Random-LOS OTA Measurement," *submitted to IEEE Transactions on Antennas and Propagation.*

[33] A. Goldsmith, *Wireless Communications.* Cambridge University Press, Aug. 2005.

[34] A. Razavi, A. A. Glazunov, P. S. Kildal, and J. Yang, "Characterizing Polarization-MIMO Antennas in Random-LOS Propagation Channels," *IEEE Access*, vol. 4, pp. 10 067–10 075, 2016.

[35] A. Paulraj, R. Nabar, and D. Gore, *Introduction to Space-Time Wireless Communications.* Cambridge University Press, May 2003.

[36] R. Haupt, "Generating a plane wave with a linear array of line sources," *IEEE Transactions on Antennas and Propagation*, vol. 51, no. 2, pp. 273–278, Feb. 2003.

[37] P.-S. Kildal, X. Chen, C. Orlenius, M. Franzén, and C. Patané, "Characterization of Reverberation Chambers for OTA Measurements of Wireless Devices: Physical Formulations of Channel Matrix and New Uncertainty Formula," *IEEE Transactions on Antennas and Propagation*, vol. 60, no. 8, pp. 3875–3891, Aug. 2012.

[38] W. C. Jakes, *Microwave Mobile Communications*, 2nd ed. New York, NY: Wiley-IEEE Press, May 1994.

[39] H. Raza, A. Hussain, J. Yang, and P.-S. Kildal, "Wideband Compact 4-Port Dual Polarized Self-Grounded Bowtie Antenna," *IEEE Transactions on Antennas and Propagation*, vol. 62, no. 9, pp. 4468–4473, Sep. 2014.

[40] M. S. Kildal, J. Kvarnstrand, J. Carlsson, A. A. Glazunov, A. Majidzadeh, and P.-S. Kildal, "Initial measured OTA throughput of 4g LTE communication to cars with roof-mounted antennas in 2d random-LOS," in *2015 International Symposium on Antennas and Propagation (ISAP)*, Nov. 2015, pp. 1–4.

[41] A. Hussain, P.-S. Kildal, and A. A. Glazunov, "Interpreting the Total Isotropic Sensitivity and Diversity Gain of LTE-Enabled Wireless Devices From Over-the-Air Throughput Measurements in Reverberation Chambers," *IEEE Access*, vol. 3, pp. 131–145, 2015.

[42] X. Chen, P.-S. Kildal, and M. Gustafsson, "Characterization of Implemented Algorithm for MIMO Spatial Multiplexing in Reverberation Chamber," *IEEE Transactions on Antennas and Propagation*, vol. 61, no. 8, pp. 4400–4404, Aug. 2013.